Res Chem Intermed (2017) 43:5625–5635
DOI 10.1007/s11164-017-2952-1

Effect of different reagents to adjust the pH on the synthesis, structure, and properties of Au/SiO_2 catalysts obtained from aqueous $HAuCl_4$

Shu Wang[1] · Jie Wang[1] · Hongxia Fang[1] · Yuchuan Zheng[1] · Changjiang Li[1]

Received: 19 December 2016 / Accepted: 8 April 2017 / Published online: 21 April 2017

Abstract We compared the structures and properties of Au/SiO_2 catalysts obtained from aqueous $HAuCl_4$ using different reagents to adjust the pH value. The speciation of aqueous $HAuCl_4$, Au colloids, and Au/SiO_2 catalysts were characterized in detail by ultraviolet–visible (UV–Vis) absorption spectroscopy, ion chromatography, dynamic light scattering (DLS) measurements, X-ray diffraction (XRD) analysis, and X-ray photoelectron spectroscopy (XPS). The catalytic activity and stability of the Au/SiO_2 catalysts in CO oxidation were also evaluated. The results show that the Au species in aqueous $HAuCl_4$ and the morphology of Au colloids were apparently affected by the solution pH, but were independent of the reagent used to adjust the pH value. The catalytic activity of Au/SiO_2 catalysts in low-temperature CO oxidation inevitably exhibited a volcano shape, depending on not only the pH value of the aqueous $HAuCl_4$, but also the specific reagent used to adjust the pH value, while the stability of the Au/SiO_2 catalysts depended only on the coexisting elements.

Keywords Au/SiO_2 catalysts · pH value · Coexisting elements

Introduction

In recent years, the application of low-temperature catalytic oxidation of CO has become very important environmentally and industrially [1–3]. Au nanocatalysts, first reported by Haruta et al. [4], represent one of the most exciting research topics, providing great developments in the field of heterogeneous catalysis. It is therefore

✉ Changjiang Li
licj@hsu.edu.cn

[1] School of Chemistry and Chemical Engineering, Huangshan University, Huangshan 245041, China

of great importance and also challenge to study the fundamentals of such complicated heterogeneous catalytic reactions [5–10]. Studies of surface science have become a successful strategy to define model catalysts effectively [11–13]. Reports on reactions catalyzed by supported Au nanoparticles have shown that they are structurally sensitivity, and that different sizes of supported Au nanoparticles exhibit different catalytic performance. Briñas et al. [14] produced size-controllable Au colloids capped with glutathione by varying the pH before reduction. They suggested the use of a polymeric nanoparticle precursor. The density and size of such Au(I) glutathione polymers are dependent on pH: the higher the pH, the more thorough the hydrolysis of $[AuCl_4]^-$, strongly affecting the loading of Au in the Au/Al_2O_3 catalyst, as reported by Grisel et al. [15]. To study the deposition–precipitation process for Au/Al_2O_3 catalysts from aqueous $HAuCl_4$, extended X-ray absorption fine structure (EXAFS) analysis was employed by Yang et al. [16], who observed that Au–Cl bonds with Au^{3+} ion were replaced by Au–OH on increasing the pH value of aqueous $HAuCl_4$. In previous study [17], we observed that such pH-dependent speciation of aqueous $HAuCl_4$ would influence the nucleation and growth of Au colloids. Although it is known that the pH value of aqueous $HAuCl_4$ is a very important factor influencing the structure and properties of Au/SiO_2 catalysts, the research into other influential factors is still lacking, particularly interelement effects.

In this work, we employed $HAuCl_4$ with different reagents to adjust the pH to similar values to prepare Au colloids and Au/SiO_2 catalysts, and compared the differences between these colloids and catalysts, which have different coexisting elements. Comparing Au/SiO_2 catalysts produced with different pH values, we found great similarity when using the same coexisting elements.

Experimental Section

The concentration of $HAuCl_4$ aqueous solution at pH 2.89, made from $HAuCl_4 \cdot 4H_2O$ (Au content, 47.8%), was measured to be 8.998×10^{-4} mol L^{-1} by inductively coupled plasma atomic emission spectrometry (ICP-AES). Four solutions with low pH values of 2.92 and 2.87 achieved by addition of NaCl (1.396×10^{-3} mol L^{-1}, 10 mL) or chlorine aqueous solution (Cl^- concentration of 1.279×10^{-3} mol L^{-1}, 10 mL) and with high pH values of 9.50 and 9.57 achieved by addition of NaOH aqueous solution (7.115×10^{-5} mol L^{-1}, 8 mL) or ammonia solution (1.0×10^{-2} mol L^{-1}, 9 mL) into 10 mL $HAuCl_4$ aqueous solution were stirred and stabilized for 4–8 days, where the pH values varied within ±0.01. A series of NaCl aqueous solutions with different concentrations (as measured by ICP-AES) were prepared and used to plot a working curve for ion chromatography of Cl^-. These four $HAuCl_4$ aqueous solutions are denoted as NaCl–$HAuCl_4$, Cl_2–$HAuCl_4$, NaOH–$HAuCl_4$, and NH_3–$HAuCl_4$, respectively.

Au colloids were produced by reducing these four aqueous $HAuCl_4$ solutions by addition of ascorbic acid (VC) after addition of sodium benzenesulfonate (SDBS) [17], denoted as NaCl–Au colloid, Cl_2–Au colloid, NaOH–Au colloid, and NH_3–Au colloid, respectively.

Au/SiO_2 catalysts were obtained in three steps. In the first step, the incipient wetness impregnation method was employed. The above four solutions with calculated amount of SiO_2 (40–120 mesh, specific surface area 390 $m^2\ g^{-1}$; Qingdao Haiyang Chemicals Company) were stirred and stabilized to obtain gold precursors. In the second step, dehydration of the four precursors at temperature of 80 °C for 12 h resulted in different solids, which were calcinated at 400 °C in air for 2 h in the third step. These catalysts are denoted as NaCl–Au/SiO_2, Cl_2–Au/SiO_2, NaOH–Au/SiO_2, and NH_3–Au/SiO_2, respectively.

A DELTA-320 pH-meter was used to measure the pH of aqueous solutions. The concentration of both $HAuCl_4$ and NaCl was measured by inductively coupled plasma atomic emission spectrometry. A UV-2450 UV–Vis spectrophotometer was employed to obtain the UV–Vis absorption spectra of various solutions. Ion chromatography was carried out on a DX-120 using an AS14 column with mobile phase of Na_2CO_3 (3.5×10^{-3} mol/L) and $NaHCO_3$ (1.0×10^{-3} mol/L) solution at flow rate of 1.2 mL min^{-1}; the data were analyzed using XPS-PEAK41 software. Aqueous solution of $HAuCl_4$ was filtered using a 0.45-μm micropore membrane before ion chromatography. A Dynapro-MS800 laser dynamic light scattering photometer was used to conduct dynamic light scattering (DLS) experiments. XRD spectra were acquired using a Philips X'PertPRO SUPER X-ray diffractometer with a Ni-filtered Cu K_α X-ray source operating at 40 kV and 50 mA. XPS measurements were performed using an ESCALAB 250 electron spectrometer with a monochromatized Al K_α excitation source ($h\nu = 1486.6$ eV).

A fixed-bed flow reactor was employed to evaluate the catalytic activity of Au/SiO_2. Au/SiO_2 (100 mg) was fed into the reaction pipe through which gas consisting of 1% CO and 99% dry air went at 20 mL/min. We calculated a space velocity of $12,000\ mL\ g_{cat}^{-1} h^{-1}$. The steady-state composition of the effluent gas was analyzed using an online GC-14C gas chromatograph ($T = 80$ °C, H_2 carrier gas at 30 mL/min) equipped with a TDX-01 column during 30 min at desired reaction temperature. The conversion of CO was evaluated according to the integrated peak areas for CO and CO_2, as follows:

$$\text{Activity} = \frac{A_{CO_2}}{A_{CO_2} + A_{CO}} \times 100\,\%,$$

where A_{CO_2} and A_{CO} are the peak area of CO and CO_2 as monitored by the GC-14C gas chromatograph.

Results and discussion

Figure 1 shows the UV–Vis absorption spectra of NaCl–$HAuCl_4$ (pH 2.92), Cl_2–$HAuCl_4$ (pH 2.87), NaOH–$HAuCl_4$(pH 9.50), and NH_3–$HAuCl_4$ (pH 9.57). The maximum absorption peak of NaCl–$HAuCl_4$ and Cl_2–$HAuCl_4$ was observed at 306 nm, which can be attributed to the two unresolved ligand (π)-to-metal (σ^*) charge transfer (LMCT) transitions in $[AuCl_4]^-$ [14], whereas no obvious absorption was observed for NaOH–$HAuCl_4$ or NH_3–$HAuCl_4$. The UV–Vis

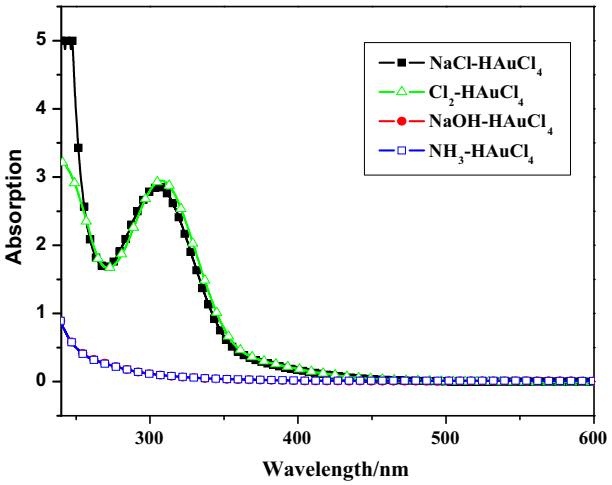

Fig. 1 UV–Vis absorption spectra of NaCl–$HAuCl_4$, Cl_2–$HAuCl_4$, NaOH–$HAuCl_4$, and NH_3–$HAuCl_4$

absorption spectra indicates that the speciation of aqueous $HAuCl_4$ changed with pH [14].

Ion chromatography was employed to quantitatively determine the speciation of NaCl–$HAuCl_4$, Cl_2–$HAuCl_4$, NaOH–$HAuCl_4$, and NH_3–$HAuCl_4$. Figure 2 shows ion chromatograms of aqueous NaCl with various Cl^- concentrations. The retention time of Cl^- was 3.8 min. A minus water peak always appears at ca. 1.88 min in the ion chromatograms. The Cl^- peak area (A) varied linearly with the Cl^- concentration ($[Cl^-]$) (Fig. 2, inset) as follows: $A = 6.279\ (\pm 0.04) \times [Cl^-] -$

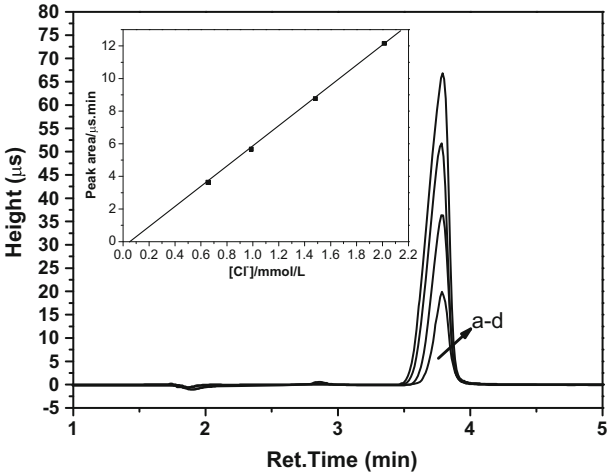

Fig. 2 Ion chromatograms with various Cl^- concentrations. Inset shows the linear dependence of the Cl^- peak area on the Cl^- concentration

0.505 (±0.06). We employed XPS PEAK41 software to fit the ion chromatogram data [17].

Figure 3 shows the ion chromatograms of NaCl–$HAuCl_4$, Cl_2–$HAuCl_4$, NaOH–$HAuCl_4$, and NH_3–$HAuCl_4$. Detailed simulation results for the ion chromatograms of NaCl–$HAuCl_4$ (A), Cl_2–$HAuCl_4$ (B), NaOH–$HAuCl_4$ (C), and NH_3–$HAuCl_4$ (D) are summarized in Table 1. Table 2 summarizes the speciation of NaCl–$HAuCl_4$ (A), Cl_2–$HAuCl_4$ (B), NaOH–$HAuCl_4$ (C), and NH_3–$HAuCl_4$ (D) and the corresponding average formula $[AuCl_x(OH)_{4-x}]^-$ ($x = 0$ to 4). These ion chromatogram results are consistent with previous reports [17], confirming the speciation of these aqueous $HAuCl_4$ solutions.

These results clearly show that the Au species in aqueous $HAuCl_4$ depend mostly on the pH value but are independent of the specific reagent used to adjust the solution pH. We studied the reduction of these four $HAuCl_4$ solutions to synthesize Au colloids. Table 3 summarizes the DLS results for the Au colloid solutions synthesized from NaCl–$HAuCl_4$, Cl_2–$HAuCl_4$, NaOH–$HAuCl_4$, and NH_3–$HAuCl_4$. These results demonstrate that the average size and homogeneity of the obtained Au colloids also depended mostly on the pH value of the aqueous $HAuCl_4$ but were independent of the specific reagent used to adjust the pH value.

The ICP-AES analysis results showed that the Au loading in the Au/SiO_2 catalysts prepared with any of the four $HAuCl_4$ solutions was the same (1.9%

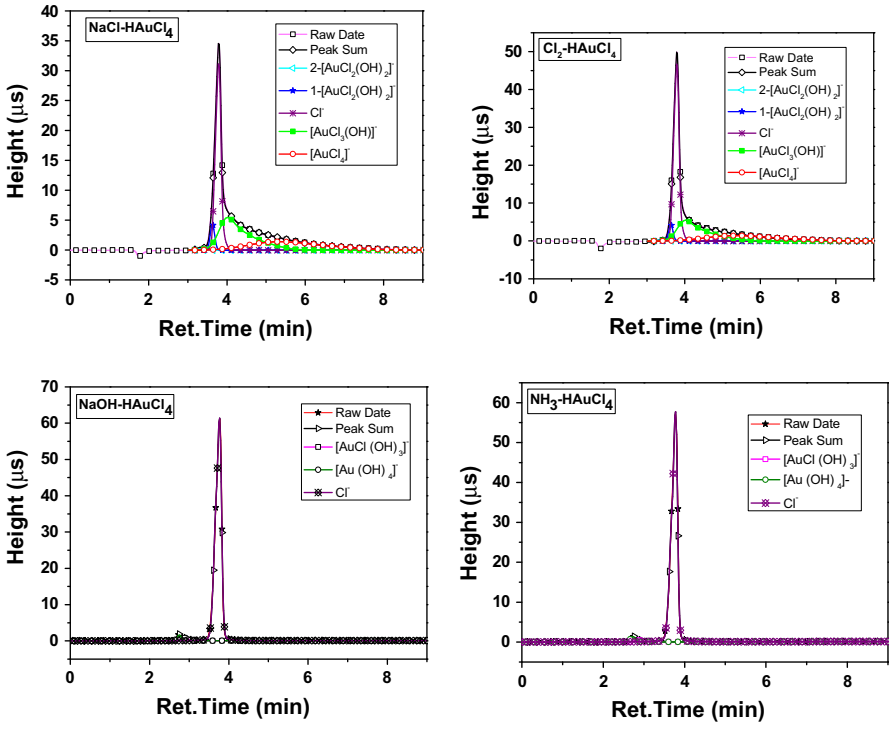

Fig. 3 Ion chromatograms of NaCl–$HAuCl_4$, Cl_2–$HAuCl_4$, NaOH–$HAuCl_4$, and NH_3–$HAuCl_4$

Table 1 Detailed simulation results of ion chromatograms of NaCl–$HAuCl_4$ (A), Cl_2–$HAuCl_4$ (B), NaOH–$HAuCl_4$ (C), and NH_3–$HAuCl_4$ (D)

	A	B	C	D
Cl^-				
Position (min)	3.80	3.80	3.80	3.80
FWHM (min)	0.17	0.16	0.16	0.16
Area (μs min)	6.76	6.48	11.65	11.04
$[AuCl_4]^-$				
Position (min)	5.43	5.43	–	–
FWHM (min)	2.23	2.20	–	–
Area (μs min)	3.52	3.48	–	–
$[AuCl_3(OH)]^-$				
Position (min)	4.04	4.04	–	–
FWHM (min)	0.95	0.95	–	–
Area (μs min)	5.20	5.22	–	–
1-$[AuCl_2(OH)_2]^-$				
Position (min)	3.66	3.66	–	–
FWHM (min)	0.14	0.15	–	–
Area (μs min)	0.64	0.65	–	–
2-$[AuCl_2(OH)_2]^-$				
Position (min)	3.34	3.34	–	–
FWHM (min)	0.13	0.14	–	–
Area (μs min)	0.031	0.032	–	–
$[AuCl(OH)_3]^-$				
Position (min)	–	–	2.90	2.90
FWHM (min)	–	–	0.24	0.23
Area (μs min)	–	–	0.19	0.10
$[Au(OH)_4]^-$				
Position (min)	–	–	2.75	2.75
FWHM (min)	–	–	0.13	0.14
Area (μs min)	–	–	0.225	0.21

FWHM, full-width at half-maximum

Table 2 Speciation of NaCl–$HAuCl_4$ (A), Cl_2–$HAuCl_4$ (B), NaOH–$HAuCl_4$ (C), and NH_3–$HAuCl_4$ (D)

	$[AuCl_x(OH)_{4-x}]^-$ (x = 0–4)					Free $[Cl^-]$ (10^{-3} mol L^{-1})	Average formula
	$x = 0$	$x = 1$	$x = 2$	$x = 3$	$x = 4$		
A	–[a]	–	+[b]	+	+	1.157	$[AuCl_{2.98}(OH)_{1.02}]^-$
B	–	–	+	+	+	1.112	$[AuCl_{2.95}(OH)_{1.05}]^-$
C	+	+	–	–	–	1.936	$[AuCl_{0.13}(OH)_{3.87}]^-$
D	+	+	–	–	–	1.839	$[AuCl_{0.12}(OH)_{3.88}]^-$

[a] Absence, [b] Presence

weight ratio). Figure 4 shows the catalytic performance of the NaCl–Au/SiO_2, Cl_2–Au/SiO_2, NaOH–Au/SiO_2, and NH_3–Au/SiO_2 in CO oxidation from the room temperature to 180 °C. As the reaction temperature increased, the catalytic activity

Table 3 DLS results of Au colloid solutions synthesized from NaCl–$HAuCl_4$, Cl_2–$HAuCl_4$, NaOH–$HAuCl_4$, and NH_3–$HAuCl_4$

Colloid	Average particle size (nm)	Polydispersity (%)
NaCl–Au colloid	16.8	18.1
Cl_2–Au colloid	15.4	17.0
NaOH–Au colloid	55.2	27.3
NH_3–Au colloid	50.1	24.7

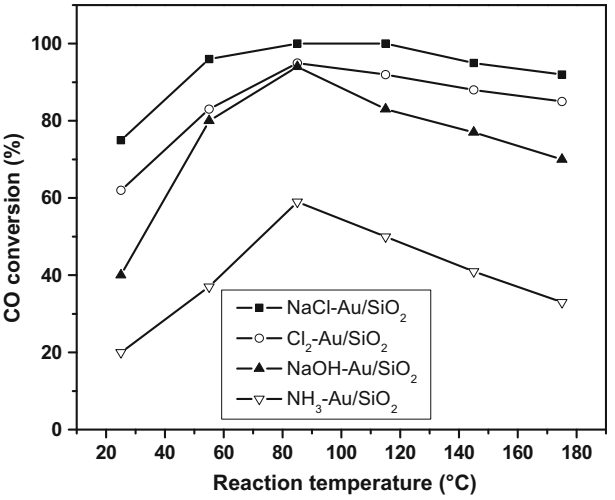

Fig. 4 Catalytic performance in CO oxidation of NaCl–Au/SiO_2, Cl_2–Au/SiO_2, NaOH–Au/SiO_2, and NH_3–Au/SiO_2

of the four catalysts first rose and then decreased. Such dependence of the catalytic activity on the reaction temperature was first found on $Au/ZnO/SiO_2$ and $Au/CeO_2/SiO_2$ catalysts [18, 19]. We considered that the conversion of CO by catalytic oxidation was co-determined by two factors: weak chemical adsorption–desorption equilibrium on the catalyst surface, and the chemical reaction on the catalyst surface, which are strongly temperature dependent. At low temperature level, increasing the temperature has little influence on the weak chemical adsorption–desorption equilibrium on the catalyst surface, while the speed of the surface chemical reaction increases dramatically. Therefore, the CO catalytic oxidation conversion rate increased as the temperature increased from low to higher values; when the temperature reached a given level, the influence of further increase on the weak chemical adsorption–desorption equilibrium can no longer be neglected, as upon reaching this level, desorption of weakly chemisorbed species occurs and eventually becomes overwhelming, so the CO catalytic oxidation conversion rate declines with further temperature increase. The CO conversion rate for NaCl–Au/

SiO_2 reached 75 and 100% at room temperature (RT) and 85 °C, respectively, indicating better catalytic performance than that for Cl_2–Au/SiO_2. Although the catalytic performance of NaOH–Au/SiO_2 was generally poorer than that of Cl_2–Au/SiO_2, they were similar at 85 °C. The conversion rate for NH_3–Au/SiO_2 was obviously poorer than for the other three catalysts. These results demonstrate that the catalytic performance of the Au/SiO_2 catalysts not only depends on the pH value of the aqueous $HAuCl_4$ but also has a close relationship with the specific reagent used to adjust the pH value.

Figure 5 displays the stability of NaCl–Au/SiO_2, Cl_2–Au/SiO_2, NaOH–Au/SiO_2, and NH_3–Au/SiO_2 in CO oxidation at 85 °C. Under the tested conditions, the CO conversion of NaCl–Au/SiO_2 and NaOH–Au/SiO_2 remained stable, whereas that of Cl_2–Au/SiO_2 and NH_3–Au/SiO_2 decreased obviously. Although the size of NaCl–Au/SiO_2 and Cl_2–Au/SiO_2 was similar, their stability differed. These results demonstrate that the stability of the Au/SiO_2 catalysts depends mostly on the coexisting elements.

Figure 6 displays the XRD patterns of NaCl–Au/SiO_2 (A), Cl_2–Au/SiO_2 (B), NaOH–Au/SiO_2 (C), and NH_3–Au/SiO_2 (D). The XRD patterns of the four catalysts all clearly show Au(111), Au(200), and Au(311) diffraction peaks. Using the Scherrer equation, the average crystalline size of Au in NaCl–Au/SiO_2 (A), Cl_2–Au/SiO_2 (B), NaOH–Au/SiO_2 (C), and NH_3–Au/SiO_2 (D) was estimated 15, 15, 20, and 22 nm, respectively. The catalytic activity and stability differed greatly between NaCl–Au/SiO_2 (A) and Cl_2–Au/SiO_2 (B) and between NaOH–Au/SiO_2 (C) and NH_3–Au/SiO_2 (D). However, the average crystalline size of the Au nanoparticles was similar, suggesting that the size of the Au nanoparticles is not the dominant factor affecting the catalytic activity and stability of these Au/SiO_2 catalysts in CO oxidation, while the effect of the coexisting elements cannot be neglected.

Figure 7 displays the Au 4*f* XPS spectra of NaCl–Au/SiO_2 (A), Cl_2–Au/SiO_2 (B), NaOH–Au/SiO_2 (C), and NH_3–Au/SiO_2 (D), while Table 4 summarizes the peak-

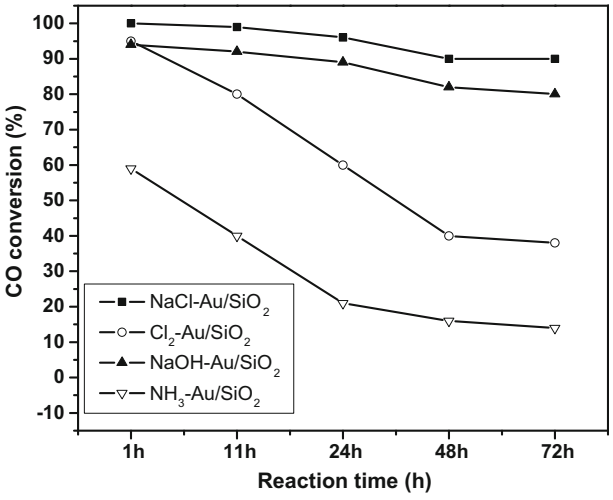

Fig. 5 Stability of NaCl–Au/SiO_2, Cl_2–Au/SiO_2, NaOH–Au/SiO_2, and NH_3–Au/SiO_2 at 85 °C

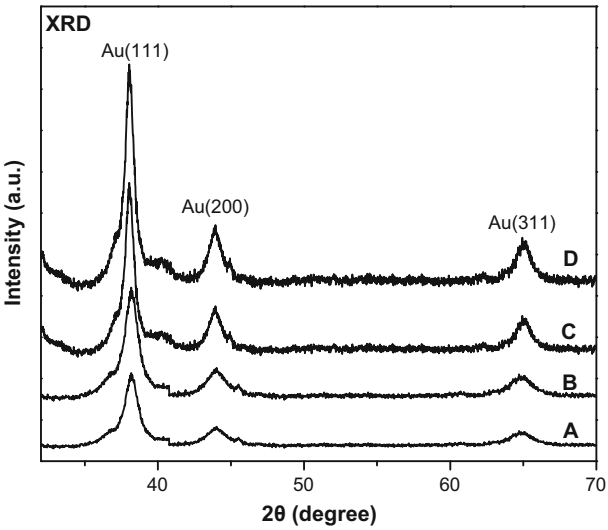

Fig. 6 XRD patterns of NaCl–Au/SiO_2 (*A*), Cl_2–Au/SiO_2 (*B*), NaOH–Au/SiO_2 (*C*), and NH_3–Au/SiO_2 (*D*)

fitting results. The Au 4*f* XPS spectrum of NaOH–Au/SiO_2 (C) could be well fit using one component centered at 84.0 eV, while the Au 4*f* XPS spectra of NaCl–Au/SiO_2 (A), Cl_2–Au/SiO_2 (B), and NH_3–Au/SiO_2 (D) consisted of two components centered at 84.0 and 84.3 eV. We attribute this upward shift of the Au 4*f* binding energy to the lower size of the Au nanoparticles. The Au nanoparticles have controllable size because we used different reagents to adjust the pH value in the previous stage.

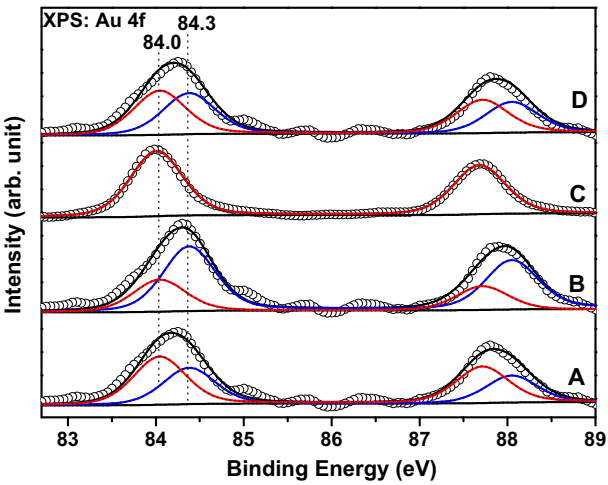

Fig. 7 XPS patterns of NaCl–Au/SiO_2 (*A*), Cl_2–Au/SiO_2 (*B*), NaOH–Au/SiO_2 (*C*), and NH_3–Au/SiO_2 (*D*). *Scattered circles* and *solid lines* indicate experimental data and fit spectra, respectively

Table 4 Peak-fitting results of Au XPS spectra of NaCl–Au/SiO_2 (A), Cl_2–Au/SiO_2 (B), NaOH–Au/SiO_2 (C), and NH_3–Au/SiO_2 (D)

Catalyst	Component 1		Component 2	
	BE (eV)	Fraction (%)	BE (eV)	Fraction (%)
A	84.0	58	84.3	42
B	84.0	35	84.3	65
C	84.0	100		
D	84.0	53	84.3	47

BE, binding energy

Conclusions

We successfully elucidated the speciation of aqueous $HAuCl_4$ with different reagents used to adjust the pH value and researched its influence on the synthesis of Au colloids and Au/SiO_2 catalysts. The Au species in aqueous $HAuCl_4$ mostly depend on the pH value and are independent of the specific reagent used to adjust the pH value. The experimental results could be grouped into two sets: A (NaCl–$HAuCl_4$), B (Cl_2–$HAuCl_4$) and C (NaOH–$HAuCl_4$), D (NH_3–$HAuCl_4$). The average formula of aqueous $HAuCl_4$ is $[AuCl_x(OH)_{4-x}]^-$, where x varies depending on the pH value ($x = 0$–4). At low pH ($\sim$2.9), x is high ($x \approx 3$), whereas for high pH ($\sim$9.5), x is low ($x \approx 0.1$). We employed aqueous $HAuCl_4$ solutions with different reagents to adjust the pH value to synthesize Au colloids and Au/SiO_2 catalysts through reduction and incipient wetness impregnation methods, respectively. The average size of the obtained Au colloids was positively correlated with the pH value of the aqueous $HAuCl_4$ and was independent of the specific reagent used to adjust the pH value. The catalytic activity and stability of the Au/SiO_2 catalysts not only depended on the pH value of the aqueous $HAuCl_4$, but was also closely related to the specific reagent used to adjust the pH value initially. The lower the electronegativity, the better the catalytic activity and stability of the Au/SiO_2 catalyst; the higher the electronegativity, the worse the catalytic activity and stability of the Au/SiO_2 catalyst. The coexisting elements should be considered in future research, as they greatly affect the catalytic activity and stability of the catalysts.

Acknowledgements This work was supported by the National Natural Science Foundation of China (21401065) and undergraduate Training Programs for Innovation, Entrepreneurship of Anhui Province (AH201310375051) and the Natural Science Foundation of Huangshan University (2011xkj014).

References

1. D. Gamarra, C. Belver, M. Fernández-García, A. Martínez-Arias, Selective CO oxidation in excess H_2 over copper-ceria catalysts: identification of active entities/species. J. Am. Chem. Soc. **129**(40), 12064–12065 (2007)
2. B.K. Min, C.M. Friend, Heterogeneous gold-based catalysis for green chemistry: low-temperature CO oxidation and propene oxidation. Chem. Rev. **107**(6), 2709–2724 (2007)
3. K. Qian, Z.X. Qian, Q. Hua, Z.Q. Jiang, W.X. Huang, Structure-activity relationship of CuO/MnO_2 catalysts in CO oxidation. Appl. Surf. Sci. **273**, 357–363 (2013)

4. M. Haruta, N. Yamada, T. Kobayashi, S. Iijima, Gold catalysts prepared by coprecipitation for low-temperature oxidation of hydrogen and of carbon monoxide. J. Catal. **115**(2), 301–309 (1989)
5. H.J. Freund, G. Pacchioni, Oxide ultra-thin films on metals: new materials for the design of supported metal catalysts. Chem. Soc. Rev. **37**, 2224–2242 (2008)
6. G. Ertl, Reactions at surfaces: from atoms to complexity (Nobel lecture). Angew. Chem. Int. Ed. **47**, 3524–3535 (2008)
7. A. Tóth, G. Halasi, F. Solymosi, Reactions of ethane with CO_2 over supported Au. J. Catal. **330**, 1–5 (2015)
8. H. Lin, J. Zheng, X.L. Zheng, Z.Q. Gu, Y.Z. Yuan, Y.H. Yang, Improved chemoselective hydrogenation of crotonaldehyde over bimetallic AuAg/SBA-15 catalyst. J. Catal. **330**, 135–144 (2015)
9. S. Chen, B.S. Zhang, D.S. Su, W.X. Huang, Titania morphology-dependent gold-titania interaction, structure, and catalytic performance of gold/titania catalysts. ChemCatChem **7**, 3290–3298 (2015)
10. J. Albadi, A. Mansournezhad, T. Sadeghi, Eco-friendly synthesis of pyrano[2,3-d]pyrimidinone derivatives catalyzed by a novel nanocatalyst of ZnO-supported copper oxide in water. Res. Chem. Intermed. **41**, 8317–8326 (2015)
11. S.A. El-Molla, G.A. Fagal, N.A. Hassan, G.M. Mohamed, Effect of the method of preparation on the physicochemical and catalytic properties of nanosized Fe_2O_3/MgO. Res. Chem. Intermed. **41**, 679–689 (2015)
12. P. Sar, A. Ghosh, B. Saha, The influence of SDS micelle on the oxidative transformation of propanol to propionaldehyde by quinquivalent vanadium in aqueous medium at room temperature. Res. Chem. Intermed. **41**, 7775–7784 (2015)
13. H.J. Freund, Model studies in heterogeneous catalysis. Chem.-A Eur. J. **16**(31), 9384–9397 (2010)
14. R.P. Briñas, M.H. Hu, L.P. Qian, E.S. Lymar, J.F. Hainfeld, Gold nanoparticle size controlled by polymeric Au (I) thiolate precursor size. J. Am. Chem. Soc. **130**(3), 975–982 (2008)
15. R.J.H. Grisel, P.J. Kooyman, B.E. Nieuwenhuys, Influence of the preparation of Au/Al_2O_3 on CH_4 oxidation activity. J. Catal. **191**(2), 430–437 (2000)
16. J.H. Yang, J.D. Henao, C. Costello, M.C. Kung, H.H. Kung, J.T. Miller, A.J. Kropf, J.G. Kim, J.R. Regalbuto, M.T. Bore, H.N. Pham, A.K. Datye, J.D. Laeger, K. Kharas, Understanding preparation variables in the synthesis of Au/Al_2O_3 using EXAFS and electron microscopy. Appl. Catal. A **291**(1–2), 73–84 (2005)
17. S. Wang, K. Qian, X.Z. Bi, W.X. Huang, Influence of speciation of aqueous $HAuCl_4$ on the synthesis, structure, and property of Au colloids. J. Phys. Chem. C **113**, 6505–6510 (2009)
18. K. Qian, W.X. Huang, J. Fang, S.S. Lv, B. He, Z.Q. Jiang, S.Q. Wei, Low-temperature CO oxidation over Au/ZnO/SiO_2 catalysts: some mechanism insights. J. Catal. **255**(2), 269–278 (2008)
19. K. Qian, J. Fang, W.X. Huang, B. He, Z.Q. Jiang, Y.S. Ma, S.Q. Wei, Understanding the deposition-precipitation process for the preparation of supported Au catalysts. J. Mol. Catal. A: Chem. **320**(1–2), 97–105 (2010)